Journal of Solid State Chemistry 183 (2010) 1354–1358

Contents lists available at ScienceDirect

Journal of Solid State Chemistry

journal homepage: www.elsevier.com/locate/jssc

Liquid–liquid interface assisted synthesis of size- and thickness-controlled Ag nanoplates

Ming-Shang Jin, Qin Kuang *, Xi-Guang Han, Shui-Fen Xie, Zhao-Xiong Xie *, Lan-Sun Zheng

State Key Laboratory for Physical Chemistry of Solid Surfaces and Department of Chemistry, College of Chemistry and Chemical Engineering, Xiamen University, Xiamen 361005, PR China

ARTICLE INFO

Article history:
Received 11 December 2009
Received in revised form
22 February 2010
Accepted 10 April 2010
Available online 27 April 2010

Keywords:
Silver
Liquid–liquid interface
Nanoplates

ABSTRACT

Here we proposed a synthetic method of high-purity Ag nanoplates by the reduction of aqueous Ag^+ ions at the aqueous–organic interface with the reductant ferrocene. We demonstrated that the as-prepared Ag nanoplates can be widely tunable from 600 nm to 7 μm in size and from 10 to 35 nm in thickness, simply by adjusting the component of organic phase. To our knowledge, there are few methods to tailor the size and the thickness of metal nanoplates in such a large range although many efforts have been made aiming to realize it. Our proposed synthetic strategy is rapid, template-free, seed-less, and high-yield, and could be applied to synthesize analogous two-dimensional nanostructures of other noble metals, such as Pt, Au, and Pd.

1. Introduction

As a kind of two-dimensional (2D) nanostructure, metal (such as Ag, Au, and Cu) nanoplates have attracted particular attention because of their special surface plasmon resonance (SPR) phenomenon in the wavelength range from visible to near-IR [1,2]. Up to date, various photo or chemical induced reduction methods have been developed to prepare metal nanoplates with different shapes [3–16]. It has been well accepted that reduction kinetics as well as shape-directing effect of the capping agents (e.g., PVP, CTAB, and PAM) play a key role in the controlled syntheses of these metal nanoplates [9–16]. But unfortunately, the synthetic strategies referred above have shown a limited control over the size (usually within 100 nm) or thickness (usually within several nanometers) of metal nanoplates. Therefore, it is desirable to explore a new and versatile route for the synthesis of metal nanoplates with a wide-range tunable size and thickness.

Interfaces, especially air–liquid interfaces and liquid–liquid interfaces, can provide a 2D constrained environment, and thus have potential applications in the organized assembly of nanocrystals. For example, Langmuir–Blodgett self-assembly happened at the air–water interface is frequently used for creating various monolayer or multilayer 2D films from nanoparticles and nanorods [17–20]. Recently, some researchers found that the use of liquid–liquid (aqueous–organic) interface could generate many nanocrystals with special shapes [21–26]. For example, Fan et al. [21] have successfully obtained pyramidal PbS nanocrystals with high-energy {113} facets at the liquid–liquid interface of toluene–water system. In addition, Sanyal and Tetsuya et al. also have succeeded in preparing Au nanosheets with the assistance of different aqueous–organic interfaces [22,23]. In comparison with the air–liquid interface, the liquid–liquid interface seems more complex, which involves many factors, such as the components and mutual solubility of two liquid phases, interfacial tensions and so on. Thus the liquid–liquid interface might provide a great opportunity to realize size- and thickness controlled synthesis of metal nanoplates in a wide range through rational interface design and condition control.

In this paper, we proposed a synthetic method of high-purity Ag nanoplates by the reduction of aqueous Ag^+ ions at the aqueous–organic interface with the reductant ferrocene. We demonstrated that the as-prepared Ag nanoplates can be widely tunable from 600 nm to 7 μm in size and from 10 to 35 nm in thickness, simply by adjusting the component of organic phase. To our knowledge, there are few methods to tailor the size and the thickness of metal nanoplates in such a large range although many efforts have been made aiming to realize it.

2. Experimental section

2.1. Chemicals and reagents

Silver nitrate ($AgNO_3$) and poly(vinyl pyrrolidone) (PVP) were purchased from Alfa Aesar. Ethanol (C_2H_5OH), toluene (C_7H_8),

* Corresponding authors. Fax: +86 592 2183047.
E-mail addresses: qkuang@xmu.edu.cn (Q. Kuang), zxxie@xmu.edu.cn (Z.-X. Xie).

0022-4596/$ - see front matter © 2010 Elsevier Inc. All rights reserved.
doi:10.1016/j.jssc.2010.04.017

n-pentanol ($C_5H_{11}OH$), methanol (CH_3OH), and cyclohexane (C_6H_{12}) were purchased from Sinopharm Chemical Regent Co. Ltd. Ferrocene ($(C_5H_5)_2Fe$) was purchased from Tianjin Guangfu Fine Chemical Research Institute. All chemicals were used as received without further purification in our experiments, and ultrapure deionized water (resistance = 18.4 MΩ cm) was used throughout the experiments.

2.2. Synthetic methods

In a typical experiment, 1 mL of an aqueous PVP solution (4 mM) and 5 mL of ethanol was sequentially added into a 25 mL beaker containing 5 mL of an aqueous $AgNO_3$ solution (6 mM) to form the aqueous phase. Then some ferrocene was dissolved into 2 mL of a toluene and n-pentanol mixed solvent (32 mM, v/v of 3:1), and the resulting solution was quickly added into the beaker as the organic phase. After the reaction for 30 min under stirring (380 rpm), some gray powders were observed in the aqueous phase. The final products were collected by centrifugation and cleaned with ethanol three times for further characterization. As listed in Table 1, the size and thickness of as-synthesized Ag nanoplates were tuned simply by adjusting the component of organic phase.

2.3. Characterization and measurements

The powder X-ray diffraction (XRD) patterns were taken from a Panalytical X'pert PRO diffractometer using Cu Ka radiation. Scanning electron microscopic (SEM) observations were carried out on a LEO1530 microscope and Hitachi S-4800 microscope. Transmission electron microscopic (TEM) and selected-area electron diffraction (SAED) measurements were carried out on JEM-2100 microscope with the accelerating voltage of 200 kV. The UV–vis spectra were recorded with a Cary 50 spectrometer (Varian).

3. Results and discussion

Scheme 1 illustrates our proposed the interface-assisted synthesis of Ag nanoplates. $AgNO_3$ as the silver source was dissolved in aqueous phase while ferrocene as the reductant was dissolved in the organic phase (such as the toluene and n-pentanol mixed solvent). Since there is an inevitable weak mutual solubility between the aqueous phase and the organic phase, the aqueous-organic interface is factually not a sharp plane but a narrow 2D region with a thickness of several nanometers [21,25]. In such a two-phase system, the reduction reaction of Ag^+ ions takes place only at the interface region due to spatial separation of reactants (Step A), and the mass transportation of Ag^+ ions are very different from that of homogenous reaction. Induced by the liquid–liquid interface, the formed silver nuclei trend to anisotropically grow up to plate-like two-dimensional Ag nanostructures (i.e., nanoplates) (Step B). Then the Ag nanoplates will penetrate the liquid–liquid interface into the aqueous phase under stirring once they are large or thick enough that their weight is over the interfacial tension (Step C). In this synthetic strategy, the anisotropic growth of Ag nanoplates is closely related with the tension of the interface region as well as the thickness of the interface (the solubility between the components in the two phases), which strongly depend on the components of aqueous–organic heterogeneous system. As a result, theoretically, the size and thickness of the as-prepared nanoplates might be tuned by adjusting the components of aqueous phase and organic phase.

To demonstrate our strategy, toluene and n-pentanol were used as the organic phase, as they are soluble each other and the reductant ferrocene can be dissolved in them. According to the previous report [27], the solubility is 0.0106 mol% for toluene in water and 0.273 mol% for water in toluene (0.375 and 3.42 mol% in the system of n-pentanol/water, respectively). Obviously, the solubility between toluene and water is much lower than that between n-pentanol and water. On the contrary, the interfacial tension of the former one is much larger than that of the latter one (36.1 dyn/m for toluene/water, and 4.4 dyn/m for n-pentanol/water) [27]. Therefore the tension and the thickness of the interface will be changed when adjusting the ratio of n-pentanol and toluene in the organic phase.

Fig. 1a is a SEM image of the product collected from the aqueous phase when the ratio of n-pentanol in the organic phase was 1/4 (i.e., the v/v ratio of toluene/n-pentanol was 3/1). Plate-like nanostructures were dominated in the product. These nanoplates owned an imperfect hexagonal or truncated triangular

Table 1
Summary of the size and thickness of silver nanoplates synthesized by the addition of n-pentanol in the toluene phase with different ratios.

Sample nos.	The organic phase (2 mL)			Average size of Ag nanoplates (μm)	Average thickness of Ag nanoplates (nm)
	Toluene	n-Pentanol	The ratio of n-pentanol		
1	2.0	0	0	0.6–0.9	35
2	1.5	0.5	1/4	1.1–1.7	30
3	1.25	0.75	3/8	1.7–3.5	15
4	1.0	1.0	1/2	**3.5–7.0**	10

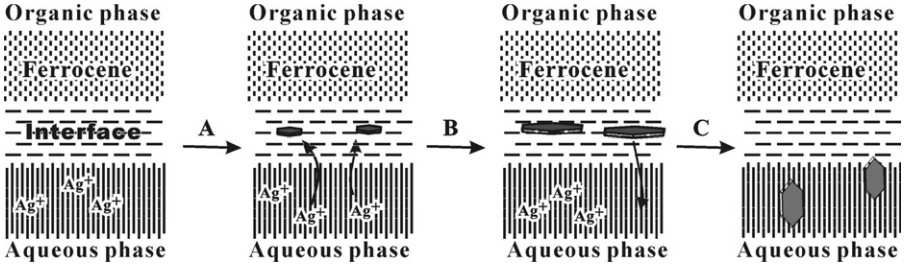

Scheme 1. Schematic illustration for the synthesis of tunable Ag nanoplates with the assistance of liquid–liquid interface.

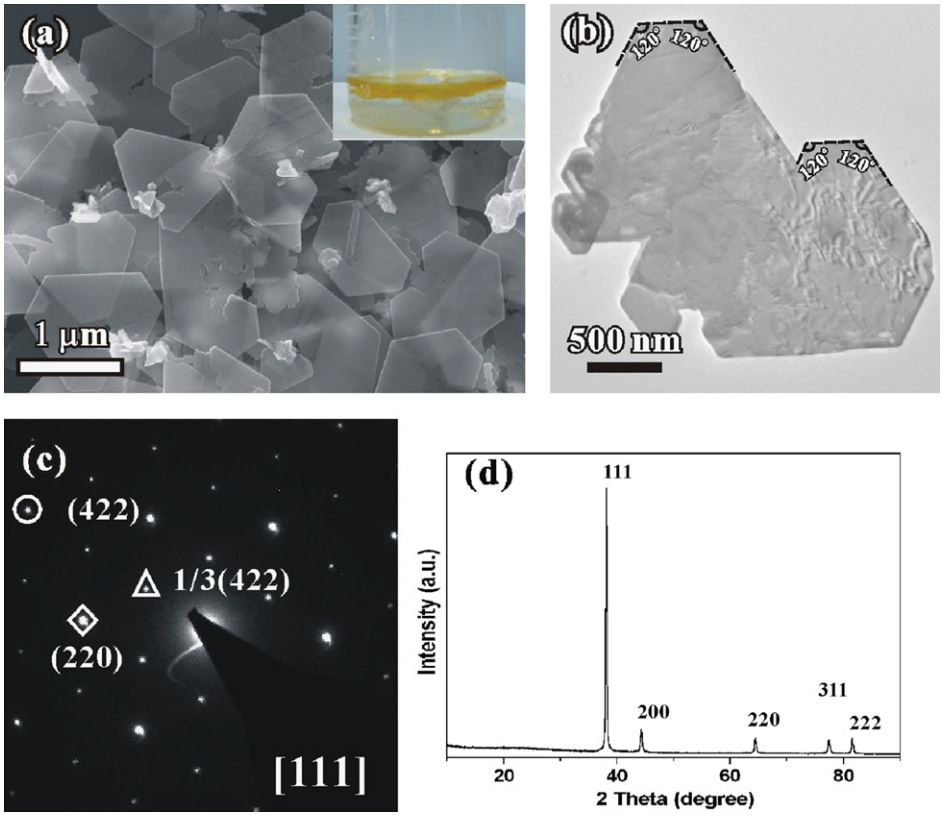

Fig. 1. (a) Low-magnification SEM image of high-purity Ag nanoplates synthesized at the ratio of n-pentanol in organic phase of 1/4. Inset is a photo of aqueous/organic interface during the synthesis; (b) high-magnification TEM image and (c) corresponding SAED pattern of a single Ag nanoplate; (d) XRD pattern of the Ag nanoplates.

geometry, which were of 1.1–1.7 μm in width, and about 30 nm in thickness. A high-magnification TEM image (Fig. 1b) of an individual hexagonal plate-like nanostructure further demonstrated that all interior angles of the nanoplate are equal to 120° although the hexagonal profile was not perfect. Fig. 1c showed the corresponding SAED pattern, which can be indexed as the diffraction along the [111] zone axis of Ag. However, 1/3{422} reflections of metal Ag with a face centered cubic (fcc) structure were observed. The appearance of the normally forbidden 1/3{422} reflections demonstrated the presence of high-intensity (111) stacking faults in thin fcc metal nanostructures [28–32]. According to the above electron microscopic data, it was concluded that the bottom/top surfaces of as-prepared Ag nanoplates are bounded by the {111} planes. Such structural characteristic of the Ag nanoplates was also reflected in the corresponding XRD pattern (Fig. 1d). The diffraction peak assigned to the {111} planes was overwhelming in intensity over the peaks arising from other planes, which deviated from the standard XRD data of the fcc-structured Ag (JCPDS no. 04-0783). The result indicates a preferential orientation of silver products with the {111} crystal plane lying parallel to the supporting substrate, being consistent to the plate feature of the silver product with the {111} planes as the bottom/top surfaces.

To demonstrate that the interface plays a key role in the formation of Ag nanoplates, the ratio of n-pentanol and toluene in the organic phase was varied, by which the tension and the thickness of the interface should be changed. Fig. 2a–d shows the SEM images of Ag products produced from different composition of the organic phase. When pure toluene solution of ferrocene was used as the organic phase, the as-obtained products were nanoplates with a size of 0.6–0.9 μm and a thickness of about 35 nm (Fig. 2a). With the increase of the ratio of n-pentanol in the organic phase, the as-obtained Ag nanoplates obviously grew larger, and reached the maximum size (up to 3.5–7.0 μm) when the ratio of n-pentanol in the organic phase was 1/2 (Fig. 2b,c). In addition, we found that the as-prepared Ag nanoplates became thinner (from 35 to 10 nm), as shown insets of Fig. 2. The size and thickness of Ag nanoplates prepared at different ratio of n-pentanol in the organic phase have been summarized in Table 1, which clearly showed the change trend of the size and thickness of the Ag nanoplates by adjusting the composition of the organic phase. Such a morphology change was accordingly reflected in corresponding XRD patterns and *UV–vis* spectra of the products (Fig. 3). As shown in Fig. 3a, with the increase of the size of Ag nanoplates, the face preference of the (111) diffraction peaks became stronger and stronger, and contrarily their width became wider and wider. At the same time, some evident SPR changes were observed in the *UV–vis* absorption spectra of the as-prepared Ag nanoplates, which can be used to monitor and recognize the size and shape of metal nanoplates [1,25,9,16,33,34]. Fig. 3b showed *UV–vis* absorption spectra for three samples synthesized by the addition of n-pentanol in the organic phase with different ratios (sample 1: pure toluene, sample 2: 1/4, and sample 3: 3/8). Both samples 1 and 2 showed a weak absorption peak at around 330 nm, and a broad absorption peak at the near-IR (centered at 780 and 950 nm, respectively). According to previous studies [1,2], the absorption peak at around 330 nm should originate from the out-of-plane quadrupole resonance of the Ag nanoplates, and the absorption peak at the near-IR should be assigned to the inplane dipole resonance, which is very sensitive to the aspect ratio of Ag nanoplates: the higher the aspect ratio of the nanoplates, the farther the location of this peak extends toward the near-IR region [5,9,16]. Therefore the red shift of the latter peak reflected the increase of the nanoplate size and the decrease of the nanoplate thickness. When Ag nanoplates is too large and too thin, the latter peak might locate at more than

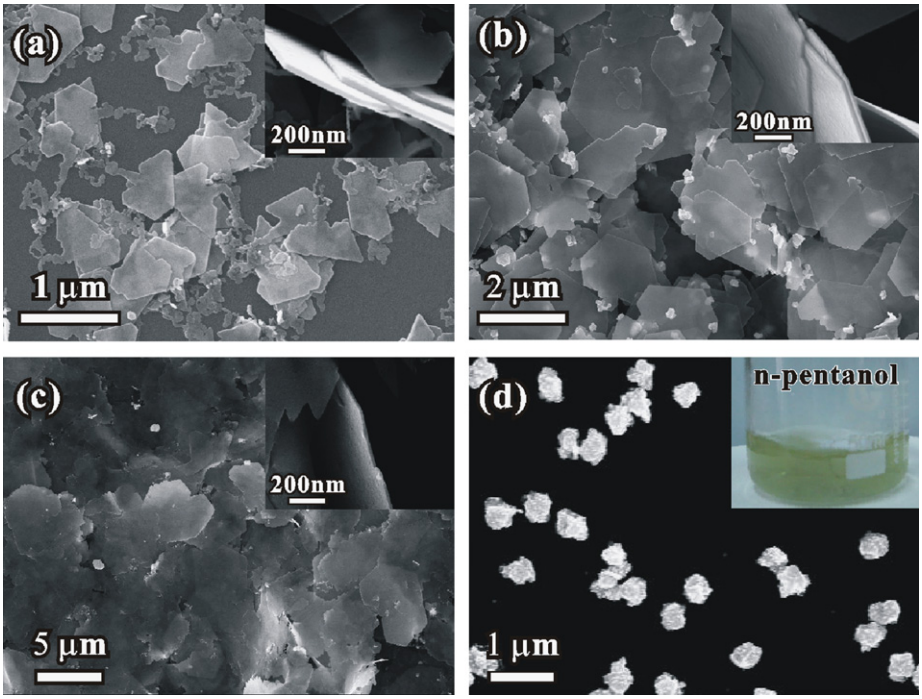

Fig. 2. SEM images of Ag nanoplates synthesized assisted by the organic–aqueous interface with different ratios of n-pentanol in the organic phase: (a) toluene only, (b) 3/8, (c) 1/2, and (d) n-pentanol only. The concentration of ferrocene in the organic phase is 32 mM and the total volume of organic phase is 2 mL. Insets in Fig. 2a, b, c are corresponding high-magnification SEM images, showing the thicknesses of as-synthesized Ag nanoplates. Inset in Fig. 2d is a photo during reaction when pure n-pentanol was used as the organic phase.

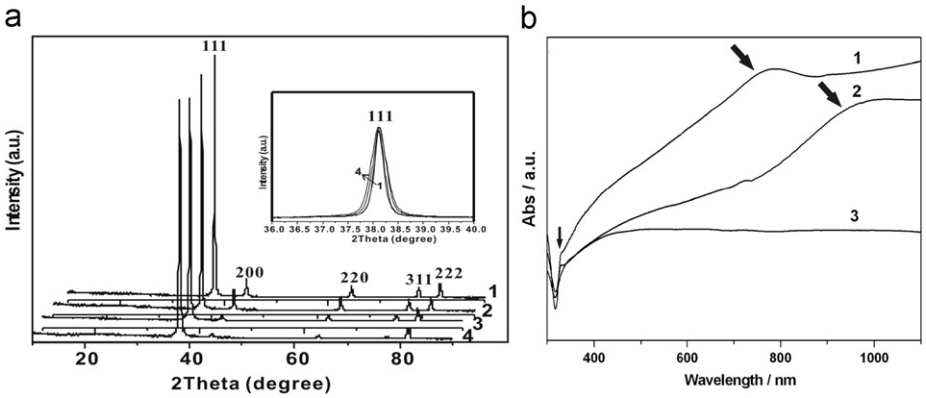

Fig. 3. (a) XRD patterns of Ag nanoplates synthesized by the addition of n-pentanol in the organic phase with different ratios: (1) pure toluene, (2) 1/4, (3) 3/8, (4) 1/2. Inset is corresponding magnified (111) diffraction peaks of the products, which was normalized to the same intensity so as to compare their full-width half-maximum (FWHM). (b) UV–vis spectra of Ag nanoplates synthesized by the addition of n-pentanol in the organic phase with different ratios: (1) pure toluene, (2) 1/4, and (3) 3/8.

1100 nm; therefore, no peak was detected in the region 300–1100 nm for sample 3.

Interestingly, we found that when pure n-pentanol solution of ferrocene was used as the organic phase, no obvious liquid–liquid interface was observed, as shown in inset of Fig. 2d. SEM observation showed that the major products at this time were no longer of a two-dimensional nanostructure, and became large numbers of irregular particles of 300–500 nm in size (Fig. 2d). This experimental phenomenon demonstrate that the interface play a key role in the formation of Ag nanoplates.

Generally, the formation of metal nanoplates is attributed to reduction kinetics as well as shape-directing effect of the capping agents, such as PVP [13–16]. In our proposed synthetic method, besides the growth kinetics, the interface rather than the capping agents plays key role in the growth of plate-like nanostructures. To demonstrate this point, we carry out the experiment for the growth of silver nanostructure in the absence of PVP by applying the same toluene/aqueous interface, and keeping other experimental conditions unchanged. The resulting Ag products show clearly to be plate-like structure, while the edges of the nanoplates are not as regular as those prepared in the presence of PVP (see Fig. 4a). Therefore, the PVP is not the key for the formation of plate-like nanostructures, but affect the lateral edge of the nanoplates. To further prove our strategy, other aqueous–organic interface systems have been applied for the synthesis of Ag nanoplates. It can be seen from Fig. 4b that analogous Ag nanoplates can be successfully synthesized at the aqueous–cyclohexane interface. On the contrary, the products obtained from aqueous–methanol system were a large number of Ag nanoleaves due to the absence of liquid–liquid interface (Fig. 4c). Based on the above experiment results, it can be concluded that the determinable condition for the formation of Ag nanoplates is the aqueous–organic liquid–liquid interface, which provides a confined 2D space for the anisotropic growth of Ag nanocrystals.

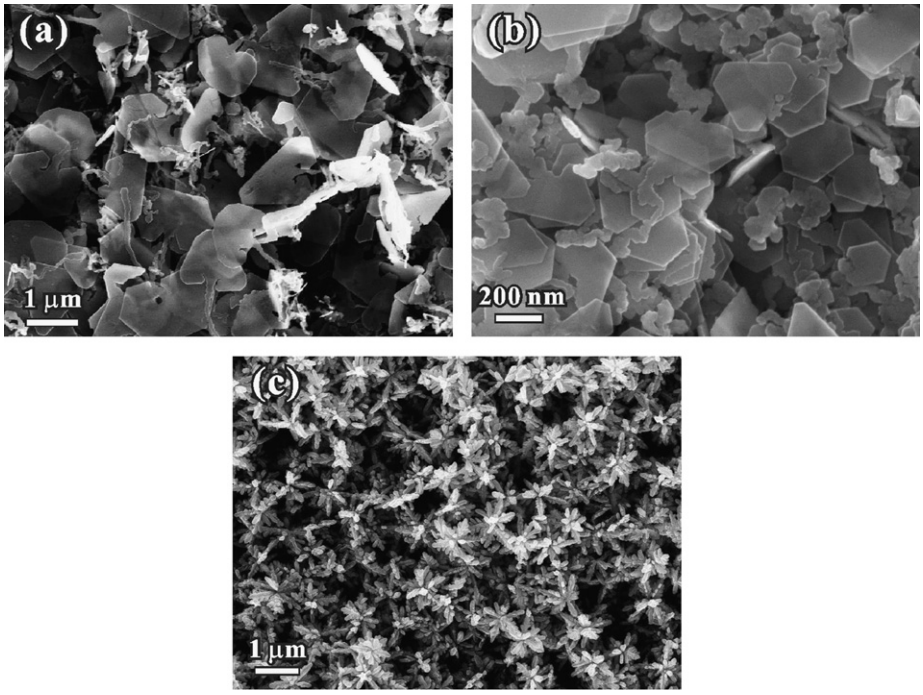

Fig. 4. (a) SEM image of silver products in the absence of PVP synthesized by the toluene/aqueous interface, (b) SEM image of silver nanoplates by using the cyclohexane/aqueous interface, and (c) SEM image of silver products by using methanol as the organic phase. See the supporting information for more experimental details.

As for the PVP, it absorbs on side surfaces of Ag nanoplates as a stabilizer and shape-directing agent, and makes them grow more regular in morphology.

4. Conclusion

In summary, we demonstrated a new method for the synthesis of Ag nanoplates with the assistant of aqueous–organic liquid–liquid interface. By rational control over the composition of the liquid–liquid interface, we realized tailoring the size and thickness of Ag nanoplates in a wide range (from 600 nm to 7 μm in size and from 10 to 35 nm in thickness). Our proposed synthetic method is rapid, template-free, seed-less, and high-yield, and it could be applied to synthesize analogous two-dimensional nanostructures of other noble metals.

Acknowledgments

This work was supported by the National Natural Science Foundation of China (Grant nos. 20725310, 20721001 and 20801045), the National Basic Research Program of China (Grant no. 2007CB815303, 2009CB939804), Key Scientific Project of Fujian Province of China (Grant no. 2009HZ0002-1).

References

[1] I. Pastoriza-Santos, L.M.J. Liz-Marzan, J. Mater. Chem. 18 (2008) 1724–1737.
[2] K.L. Kelly, E. Coronado, L.L. Zhao, G.C. Schatz, J. Phys. Chem. B 107 (2003) 668–677.
[3] R.C.Y. Jin, W. Cao, C.A. Mirkin, K.L. Kelly, G.C. Schatz, J.G. Zheng, Science 294 (2001) 1901–1903.
[4] X.L. Tian, K. Chen, G.Y. Cao, Mater. Lett. 60 (2006) 828–830.
[5] J. An, B. Tang, X.H. Ning, J. Zhou, S.P. Xu, B. Zhao, W.Q. Xu, C. Corredor, J.R. Lombardi, J. Phys. Chem. C 111 (2007) 18055–18059.
[6] T.C.R. Rocha, H. Winnischofer, E. Westphal, D. Zanchet, J. Phys. Chem. C 111 (2007) 2885–2891.
[7] H.Y. Jia, J.B. Zeng, J. An, W. Song, W.Q. Xu, B. Zhao, Thin Solid Films 516 (2008) 5004–5009.
[8] M. Maillard, P.R. Huang, L. Brus, Nano Lett. 3 (2003) 1611–1615.
[9] X.Q. Zou, E.B. Ying, H.J. Chen, S.J. Dong, Colloid Surf. A 303 (2007) 226–234.
[10] Y.J. Xiong, A.R. Siekkinen, J.G. Wang, Y.D. Yin, M.J. Kim, Y.N. Xia, J. Mater. Chem. 17 (2007) 2600–2602.
[11] I. Pastoriza-Santos, L.M. Liz-Marzan, Nano Lett. 2 (2002) 903–905.
[12] S.H. Chen, D.L. Carroll, J. Phys. Chem. B 108 (2004) 5500–5506.
[13] J. Zou, Y. Xu, B. Hou, D. Wu, Y. Sun, China Particuology 5 (2007) 206–212.
[14] Y.A. Sun, Y.N. Xia, Adv. Mater. 15 (2003) 695–699.
[15] Y.G. Sun, B. Mayers, Y.N. Xia, Nano Lett. 3 (2003) 675–679.
[16] I. Washio, Y.J. Xiong, Y.D. Yin, Y.N. Xia, Adv. Mater. 18 (2006) 1745–1749.
[17] K. Kim, H.B. Lee, J.W. Lee, H.K. Park, K.S. Shin, Langmuir 24 (2008) 7178–7183.
[18] K.Y. Lee, M.J. Kim, J. Hahn, J.S. Suh, I.Y. Lee, K. Kim, S.W. Han, Langmuir 22 (2006) 1817–1821.
[19] C. Liu, Y.J. Li, M.H. Wang, Y. He, E.S. Yeung, Nanotechnology 20 (2009) 1–6.
[20] A.R. Tao, J.X. Huang, P.D. Yang, Acc. Chem. Res. 41 (2008) 1662–1673.
[21] D.B. Fan, P.J. Thomas, P. O'Brien, J. Am. Chem. Soc. 130 (2008) 10892–10894.
[22] A. Sanyal, M. Sastry, Chem. Commun. (2003) 1236–1237.
[23] T. Kida, Langmuir 24 (2008) 7648–7650.
[24] K.Y. Lee, M. Kim, S.W. Han, Mater. Lett. 63 (2009) 480–482.
[25] C.N.R. Rao, K.P. Kalyanikutty, Acc. Chem. Res. 41 (2008) 489–499.
[26] C.N.R. Rao, G.U. Kulkarni, V.V. Agrawal, U.K. Gautam, M. Ghosh, U. Tumkurkar, J. Colloid Interf. Sci. 289 (2005) 305–318.
[27] A.H. Demond, A.S. Lindner, Environ. Sci. Technol. 27 (1993) 2318–2331.
[28] V. Germain, J. Li, D. Ingert, Z.L. Wang, M.P. Pileni, J. Phys. Chem. B 107 (2003) 8717–8720.
[29] S.H. Zhang, Z.Y. Jiang, Z.X. Xie, X. Xu, R.B. Huang, L.S. Zheng, J. Phys. Chem. B 109 (2005) 9416–9421.
[30] A.I. Kirkland, D.A. Jefferson, D.G. Duff, P.P. Edwards, Inst. Phys. Conf. Ser. 98 (1990) 375–378.
[31] S.H. Chen, D.L. Caroll, Nano Lett. 2 (2002) 1003–1007.
[32] C. Lofton, W. Sigmund, Adv. Funct. Mater. 15 (2005) 1197–1208.
[33] M. Popa, T. Pradell, D. Crespo, J.M. Calderón Moreno, Colloid Surf. A: Physicochem. Eng. Aspects 303 (2007) 184–190.
[34] V. Torres, M. Popa, D. Crespo, J.M. Calderón Moreno, Microelectron. Eng. 84 (2007) 1665–1668.